Magnetic Resonance in Medicine

Microscopic theory of spin–spin and spin–lattice relaxation of bound protons in cellular and myelin membranes—A lateral diffusion model (LDM)

Alexander L. Sukstanskii | Dmitriy A. Yablonskiy

Department of Radiology, Washington University in Saint Louis, Saint Louis, Missouri, USA

Correspondence
Dmitriy A. Yablonskiy, Mallinckrodt Institute of Radiology, Washington University, 4525 Scott Ave. Room 3216 St. Louis MO, 63110.
Email: yablonskiyd@wustl.edu

Purpose: Deciphering salient features of biological tissue cellular microstructure in health and diseases is an ultimate goal of MRI. While most MRI approaches are based on studying MR properties of tissue "free" water indirectly affected by tissue microstructure, other approaches, such as magnetization transfer (MT), directly target signals from tissue-forming macromolecules. However, despite three-decades of successful applications, relationships between MT measurements and tissue microstructure remain elusive, hampering interpretation of experimental results. The goal of this paper is to develop microscopic theory connecting the structure of cellular and myelin membranes to their MR properties.

Theory and Methods: Herein we introduce a lateral diffusion model (LDM) that explains the T_2 (spin–spin) and T_1 (spin–lattice) MRI relaxation properties of the macromolecular-bound protons by their dipole–dipole interaction modulated by the lateral diffusion of long lipid molecules forming cellular and myelin membranes.

Results: LDM predicts anisotropic T_1 and T_2 relaxation of membrane-bound protons. Moreover, their T_2 relaxation cannot be described in terms of a standard $R_2 = 1/T_2$ relaxation rate parameter, but rather by a relaxation rate function $R_2(t)$ that depends on time t after RF excitation, having, in the main approximation, a logarithmic behavior: $R_2(t) \sim \ln t$. This anisotropic non-linear relaxation leads to an absorption lineshape that is different from Super-Lorentzian traditionally used in interpreting MT experiments.

Conclusion: LDM-derived analytical equations connect the membrane-bound protons T_1 and T_2 relaxation with dynamic distances between protons in neighboring membrane-forming lipid molecules and their lateral diffusion. This sheds new light on relationships between MT parameters and microstructure of cellular and myelin membranes.

KEYWORDS
bound protons, lateral diffusion, MRI, MT, spin–spin and spin–lattice relaxation, tissue microstructure

1 | INTRODUCTION

NMR imaging is a powerful tool for analyzing structure and functioning of human and animal brains in health and disease. Relaxation (R_1, R_2, R_2^*, etc.,), diffusion, magnetic susceptibility and magnetization transfer (MT) parameters are among the most important and broadly used metrics characterizing brain tissue, where these parameters differ from those in pure water due to strong interaction between hydrogen protons of water and macromolecules (lipids, proteins, etc.) forming biological tissue cellular structure. These differences are especially pronounced in a so-called myelin water (MW), that is, water trapped between lipid bilayers forming myelin sheath around axons, where the surface-to-volume ratio for interaction between water and macromolecules is very high and, therefore, the strength of the interaction effects is substantially elevated.

A theoretical analysis describing the influence of macromolecules on water proton relaxation and MT properties is usually based on multi-compartment models. In a simplest two-compartment model, one of the compartments (often-called free water or free pool) representing a combination of intra- and extra-cellular water, and another compartment (usually called bound pool) representing protons bound to macromolecules. Direct experiments with the myelin extracts and myelinated nerves[1,2] revealed that the bound pool represents mostly long-chain methylene protons. This bound pool protons are characterized by a very short transverse magnetization decay time T_2 in the range of 10 microseconds, making this compartment "invisible" in conventional MR experiments. However, interaction of the bound protons with the free water compartment, makes it possible to indirectly detect protons bound to macromolecules in MT experiments with off-resonance single[3–5] and double[6] excitation pulses (see recent reviews[7,8] and numerous references therein), as well as with on-resonance RF pulses.[9–14] Recent development of in vivo ultra-short TE techniques, also demonstrated the presence of the components with T_2^* in a sub-millisecond range.[15–17] While MT-base approaches found rather broad applications for studying different diseases (see discussion in Refs.[7,8]), microscopic mechanisms relating actual microstructure and dynamics of macromolecules within myelin sheath to transverse relaxation properties of bound protons remain largely unknown.[18]

In the present study, we introduce a lateral diffusion model (LDM) that explains the T_2 (spin–spin) and T_1 (spin–lattice) MRI relaxation properties of the macromolecular-bound protons by their dipole–dipole interaction modulated by the lateral diffusion of long lipid molecules forming cellular and myelin membranes. We demonstrate that the transverse relaxation properties of the bound protons in the myelin layers can be explained in the framework of the model accounting for their spin–spin interaction modulated by the lateral diffusion of long lipid molecules in the bilayers forming cellular membranes and myelin sheath. We also show that, the modulation of spin–lattice interaction of bound protons by the lateral diffusion of long lipid molecules can substantially contribute to their T_1 relaxation processes, thus complementing previously discuss rotational mechanisms[19] and the recent study,[20] where the dipolar induced spin–lattice relaxation between water and bound protons in the myelin sheath was numerically investigated by using a computer-simulated atomistic model of the myelin sheath with a realistic lipid composition.

Our results show that the decay of the transverse magnetization component $M_\perp(t)$ associated with the bound protons in the bilayers forming myelin sheath is highly anisotropic, and its time dependence differs from either Lorentzian (linear exponential) or Gaussian (quadratic exponential). Instead, the LDM presented here leads to the following expression for the transverse magnetization of the bilayer-bound protons:

$$M_\perp(t) = M_\perp(0) \cdot \exp\left[-R_2(t,\alpha) \cdot t\right] \quad (1)$$

with a transverse *relaxation rate function* $R_2(t,\alpha)$ (an analog of a common t-independent transverse relaxation rate parameter) that depends on the time t after excitation pulse and the local orientation (α) of the main axis of the lipid chains in the bilayers with respect to the magnetic field $\mathbf{B}_0$ (see Figure 1). For experimentally realistic measurement times, t is much longer than the characteristic diffusion time τ_d of bound protons (which is in a sub-microsecond range as defined by Equation (31) below), and $R_2(t,\alpha)$ of the bilayer-bound protons can be presented as follows:

$$R_2(t,\alpha) = \lambda \cdot \left\{ \left(1 - 3\cos^2\alpha\right)^2 \right.$$
$$\left. \cdot \left[\ln\left(\frac{t}{\tau_d}\right) - \kappa_0 + 4 \cdot \left(\frac{\pi\tau_d}{t}\right)^{1/2}\right] + \kappa_2 \cdot \sin^4\alpha \right\} \quad (2)$$

where numerical coefficients κ_0 and κ_2 ($\kappa_0 = 3.20$, $\kappa_2 = 0.75$), as well as the parameter λ (Equation (20) below) are the LDM-defined parameters depending on the spin–spin interactions. In the opposite limit, that is, for small times t, $R_2(t,\alpha) \to 0$. Such a dependence of the bilayer-bound protons $R_2(t,\alpha)$ on the time t after excitation leads to their lineshape that cannot be described by either Lorentzian
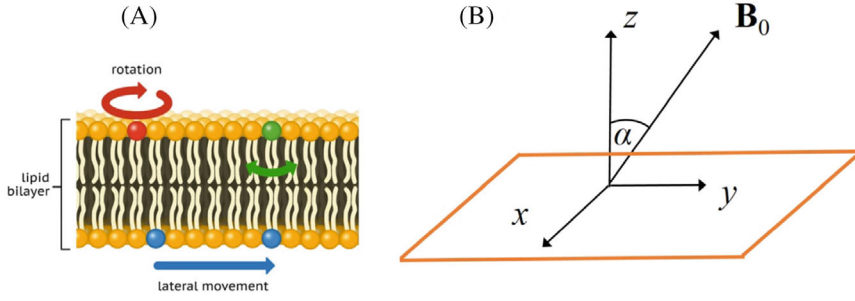
FIGURE 1 A, A simplified schematic structure of the lipid bilayer; light yellow lines represent lipid molecules within the bilayer, oriented along the normal to the layer (axis z). B, The geometry of the 2D system under consideration. The external field $\mathbf{B}_0$ lays in the (yz) plane and makes an angle α with the normal to the layer. The molecules diffuse in the (xy) plane preserving positions of their elements (including methylene protons) along the z direction.

or Gaussian shape-functions. In fact, for large frequency shifts $\Delta\omega \cdot T_2 > 1$ usually used in MT experiments, the LDM lineshape of the bilayer-bound protons can be presented as

$$L(\Delta\omega, \alpha) = \frac{\Lambda(\Delta\omega, \alpha)}{\Delta\omega^2} \qquad (3)$$

where

$$\Lambda(\Delta\omega, \alpha) = \frac{\lambda}{2} \cdot \left\{ \left(1 - 3\cos^2\alpha \right)^2 \cdot \left[\ln\left(\frac{\pi}{4 \cdot \Delta\omega \cdot \tau_d} \right) \right. \right.$$
$$\left. \left. - \kappa_0 + \kappa_1 \cdot (\Delta\omega \cdot \tau_d)^{1/2} \right] + \kappa_2 \cdot \sin^4\alpha \right\} \quad (4)$$

with an additional numerical constant $\kappa_1 = 12 - 4\sqrt{2}$. Equations (2)–(4) show a significant anisotropy of signal transverse relaxation and the corresponding lineshape function that reflects anisotropy of the lipid structure and the membrane orientation.

While results presented above provide information on protons' spin–spin relaxation in "flat" bilayers (as shown in Figure 1), in biological tissues these bilayers are organized in cellular membranes and myelin sheath. For a bundle of parallel axons (i.e., white matter [WM] tracks) with the main axis tilted by an angle β with respect to the external magnetic field $\mathbf{B}_0$, the LDM expression for the axonal bundle lineshape for large frequency shifts $\Delta\omega \cdot T_2 > 1$ becomes as follows:

$$L_{axon}(\Delta\omega, \ \beta) = \frac{\lambda}{2(\Delta\omega)^2} \cdot \left\{ \left[\ln\left(\frac{\pi}{4\,\Delta\omega \cdot \tau_d} \right) \right. \right.$$
$$\left. - \kappa_0 + \kappa_1 \cdot (\Delta\omega \cdot \tau_d)^{1/2} \right] \cdot \left(\frac{27}{8} \left(\cos^2\beta - \frac{5}{9} \right)^2 + \frac{1}{3} \right) +$$
$$\left. + \kappa_2 \cdot \left(\cos^2\beta + \frac{3}{8} \cdot \sin^4\beta \right) \right\} \qquad (5)$$

For randomly oriented membranes (as usually assumed in MT experiments describing WM axonal structure), the global LDM lineshape function for large frequency shifts,

$\Delta\omega \cdot T_2 > 1$, can be presented as follows:

$$\overline{L}(\Delta\omega) = \frac{2\lambda}{5(\Delta\omega)^2} \cdot \left\{ \ln\left(\frac{\pi}{4\,\Delta\omega \cdot \tau_d} \right) \right.$$
$$\left. + \kappa_1 \cdot (\Delta\omega \cdot \tau_d)^{1/2} - \kappa_0 + \frac{2}{3}\kappa_2 \right\} \qquad (6)$$

For an arbitrary frequency shift $\Delta\omega$, the LDM lineshapes can be approximated by an interpolation formula given in Equation (37).

A list of all notations used in this paper is provided in the Appendix.

2 | THEORY

2.1 | LDM

Myelin sheath is a multilamellar membrane surrounding the axons of neurons in central and peripheral nerve systems. It consists of repeating units of double bilayers separated by aqueous layers that alternate between the cytoplasmic and extracellular fluid content. Each bilayer comprises long lipid and protein molecules[21–23] with the long axis oriented mostly perpendicular to the bilayer's surface. The MR spectrum of myelin lipids is dominated by the alkyl chain methylene groups.[1,2] Importantly, proton mobility in proton-carrying lipid molecules is highly restricted along their long axes, whereas these proton-carrying lipids can diffuse laterally in the xy-plane (see Figure 1). Experiments in model bilayer systems revealed that the corresponding lateral diffusion coefficient D varies in the range of $10^{-4} - 10^{-2} \ \mu m^2/msec$, depending on the bilayer-forming lipids and the experimental settings. For example, Schoch et al[24] reported $D \sim 0.8 \cdot 10^{-4} - 4 \cdot 10^{-3} \ \mu m^2/msec$ for supported lipid bilayers and $D \sim 13 \cdot 10^{-3} - 20 \cdot 10^{-3} \ \mu m^2/msec$ for free-floating bilayers. Quite a few other studies also reported D for model bilayer systems in the range of $10^{-4} - 10^{-2} \ \mu m^2/msec$ (e.g.,[25–31]). Hence, the motion of

lipid-bound protons can be considered as a lateral 2D diffusion, which is accompanied by lipid molecule rotation (Figure 1). Importantly, for the range of diffusion coefficients $10^{-4} - 10^{-2} \, \mu m^2/\text{msec}$, the diffusion component of motion leads to the spin–spin correlation times on the order of nanoseconds, while the rotation times are much faster – in the picosecond range[32] making their contribution to the relaxation processes smaller than the diffusion-mediated interaction between spins. Accordingly, in this paper we focus only on the diffusion processes and their contribution to the spin–spin (T_2) and spin–lattice (T_1) relaxation of lipid-bound protons.

The very short correlation time along with the rapid decrease of the dipole–dipole interaction with a distance between dipoles makes it possible, as the first approximation, to account for interactions only between protons located at the planes with the same z-coordinate. Note also that in the application to the myelin sheath or lipid cellular membranes, their curvature can be ignored because the distance between neighboring lipid chains is on the order of Angstroms, while the radii of the myelin sheath or membranes are significantly bigger–in the µm scale. A schematic simplified structure of the lipid bilayer and the geometry of the system under consideration is depicted in Figure 1.

3 | METHODS

According to the classical theory of dipole–dipole relaxation,[33,34] the dipole–dipole interaction of uncorrelated identical spins results in the following expressions for the relaxation parameters $R_{1,2} = 1/T_{1,2}$:

$$R_1 = \frac{3}{2} \cdot \left(\hbar \gamma^2 \right)^2 \cdot I(I+1) \cdot \left\{ J^{(1)}(\omega) + J^{(2)}(2\omega) \right\} \quad (7)$$

$$R_2 = \frac{3}{8} \cdot \left(\hbar \gamma^2 \right)^2 \cdot I(I+1)$$
$$\cdot \left\{ J^{(0)}(0) + 10 \cdot J^{(1)}(\omega) + J^{(2)}(2\omega) \right\} \quad (8)$$

where $\hbar$ is the Planck constant, γ is the gyromagnetic ratio, I is the nuclear spin (1/2 in our case), $\omega = \gamma B_0$ is the Larmor frequency in the external magnetic field B_0. The spectral densities $J^{(m)}(\omega)$ ($m = 0, 1, 2$) are the Fourier transforms of the correlation functions $G^{(m)}(\tau)$:

$$J^{(m)}(\omega) = \int_{-\infty}^{\infty} d\tau \; G^{(m)}(\tau) \cdot e^{-i\omega\tau}$$
$$G^{(m)}(\tau) = \overline{F^{(m)}(t) \cdot F^{(m)*}(t+\tau)} \quad (9)$$

The upper bar means averaging over positions and orientations of the dipoles. The factors $F^{(m)}$ depend on the vector $\mathbf{r}$ between two dipoles:

$$F^{(0)} = \frac{1 - 3 \cdot \cos^2\theta}{r^3}, \quad F^{(1)} = \frac{\sin\theta \cdot \cos\theta}{r^3} \cdot e^{-i\varphi},$$
$$F^{(2)} = \frac{\sin^2\theta}{r^3} \cdot e^{-2i\varphi} \quad (10)$$

where (r, θ, φ) are the distance, polar and azimuthal angles of the vector $\mathbf{r}$ in the spherical coordinates with the polar axis along the external field $\mathbf{B}_0$.

Assuming random lateral diffusion of spins and using Equation (10), the correlation functions $G^{(m)}(\tau)$ can be presented in the form:

$$G^{(m)}(\tau) = \frac{n_2}{(8\pi D\tau)} \cdot \iint d\boldsymbol{\rho}_1 \, d\boldsymbol{\rho}_2 \frac{p_m(\theta_1, \varphi_1) \cdot p_m^*(\theta_2, \varphi_2)}{\rho_1^3 \cdot \rho_2^3}$$
$$\cdot \exp\left[-\frac{(\boldsymbol{\rho} - \boldsymbol{\rho}_0)^2}{8D\tau} \right] \quad (11)$$

where n_2 is the spins' surface density (number of spins per unit area of 2D plane), D is the lateral diffusion coefficient, and

$$p_0(\theta, \varphi) = 1 - 3 \cdot \cos^2\theta$$
$$p_1(\theta, \varphi) = \sin\theta \cdot \cos\theta \cdot \exp(-i\varphi)$$
$$p_2(\theta, \varphi) = \sin^2\theta \cdot \exp(-2i\varphi) \quad (12)$$

The integrals in Equation (11) should be taken over the regions $\rho_{1,2} \geq d$, where d is a minimal "approachable" distance between dipoles.[33,34]

The angles θ and φ entering Equations (12) are related to the angle α and the azimuthal angle ψ in the xy plane (see Figure 1) as follows:

$$\cos\theta = -\sin\psi \cdot \sin\alpha$$
$$\sin\theta \cdot e^{-i\varphi} = \cos\psi - i \cdot \sin\psi \cdot \cos\alpha \quad (13)$$

After a series of tedious but straightforward transformations, the following expression for the correlation functions can be obtained:

$$G^{(m)}(\tau) = \frac{n_2\pi}{4d^4} \cdot \left[v_0^{(m)}(\alpha) \cdot \Psi_0(\varepsilon) + v_2^{(m)}(\alpha) \cdot \Psi_2(\varepsilon) \right]$$
$$\Psi_{0,2}(\varepsilon) = \int_0^{\infty} x^3 dx \cdot \exp\left(-\varepsilon \cdot x^2 \right) \cdot \psi_{0,2}^2(x) \quad (14)$$

$$\psi_0(x) = \frac{1}{2} \cdot \left[-2 + J_1(x) \cdot (-2 + \pi x \cdot \mathbf{H}_0(x)) \right.$$
$$\left. + \frac{J_0(x)}{x} \cdot \left(2 + 2x^2 - \pi x^2 \cdot \mathbf{H}_1(x) \right) \right]$$

$$\psi_2(x) = \frac{1}{3x^2} \cdot \left[x^2 - x \cdot \left(1 + x^2\right) \cdot J_0(x) + \left(2 + x^2\right) \cdot J_1(x) \right] -$$
$$- \frac{\pi x}{6} \cdot \left[J_0(x) \cdot \mathbf{H}_1(x) - J_1(x) \cdot \mathbf{H}_0(x) \right] \quad (15)$$

where $J_{0,1}(x)$ and $\mathbf{H}_{0,1}(x)$ are the Bessel and Struve functions, respectively, $\varepsilon = \tau/\tau_d$, $\tau_d = d^2/2D$ is the characteristic diffusion time. The angle-dependent coefficients $v_{0,2}^{(m)}(\alpha)$ in Equation (14) are

$$v_0^{(0)}(\alpha) = \left(1 - 3\cos^2 \alpha\right)^2, \quad v_0^{(1)}(\alpha) = \sin^2 \alpha \cdot \cos^2 \alpha,$$
$$v_0^{(2)}(\alpha) = \sin^4 \alpha$$
$$v_2^{(0)}(\alpha) = \frac{9}{2} \cdot \sin^4 \alpha, \quad v_2^{(1)}(\alpha) = \frac{1}{2} \cdot \sin^2 \alpha \cdot \left(1 + \cos^2 \alpha\right)$$
$$v_2^{(2)}(\alpha) = \frac{1}{2} \cdot \left(8 \cdot \cos^2 \alpha + \sin^4 \alpha\right) \quad (16)$$

The relaxation parameters are defined by the spectral densities $J^{(m)}(\omega)$, Equations (7) and (8). Substituting $G^{(m)}(\tau)$ in Equation (9), we get

$$J^{(m)}(\omega) = \frac{n_2 \pi}{4 D d^2} \cdot \left[v_0^{(m)}(\alpha) \cdot V_0(\Omega) + v_2^{(m)}(\alpha) \cdot V_2(\Omega) \right] \quad (17)$$

where $\Omega = \omega \cdot \tau_d$ and the functions $V_{0,2}(\Omega)$ are

$$V_{0,2}(\Omega) = \int_0^\infty dx \; \phi_{0,2}(x, \; \Omega),$$
$$\phi_{0,2}(x, \; \Omega) = \psi_{0,2}^2(x) \cdot \frac{x^5}{\left(x^4 + \Omega^2\right)} \quad (18)$$

4 | RESULTS

4.1 | Spin–Lattice (Longitudinal) Relaxation of Bound Protons in Lipid Bilayers

Combining Equations (7) and (17), the longitudinal (spin–lattice) relaxation rate parameter R_1 can be presented as follows:

$$R_1 = 8\lambda \cdot \left[\sin^2 \alpha \cdot \cos^2 \alpha \cdot V_0(\Omega) + \sin^4 \alpha \cdot V_0(2\Omega) + \right.$$
$$+ \frac{1}{2} \cdot \sin^2 \alpha \cdot \left(1 + \cos^2 \alpha\right) \cdot V_2(\Omega) +$$
$$\left. \frac{1}{2} \cdot \left(8 \cdot \cos^2 \alpha + \sin^4 \alpha\right) \cdot V_2(2\Omega) \right] \quad (19)$$

where $\Omega = \omega \cdot \tau_d$, the functions $V_{0,2}(\Omega)$ are defined in Equation (18), and

$$\lambda = \frac{9\pi \cdot n_2}{256 \cdot D \cdot d^2} \cdot \left(\hbar \gamma^2\right)^2 \quad (20)$$

The functions $V_{0,2}(\Omega)$ are illustrated in Figure 2. The inset demonstrates $V_{0,2}(\Omega)$ at small values of Ω.
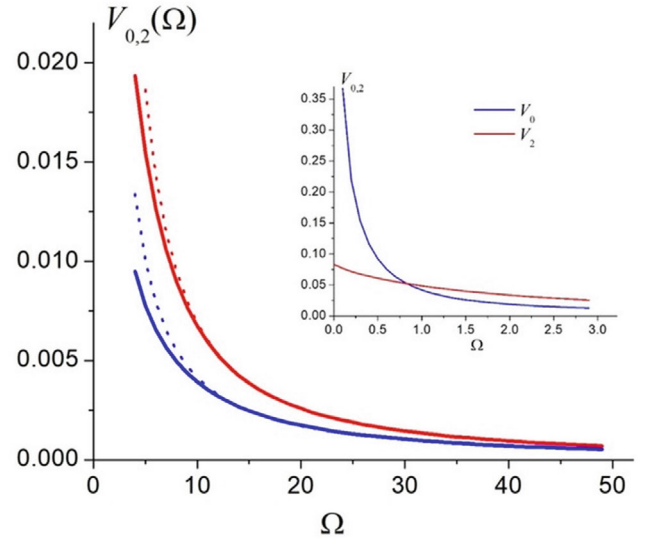

FIGURE 2 The functions $V_{0,2}(\Omega)$ (solid lines). The dashed lines show approximations describing $V_{0,2}(\Omega)$ functions for $\Omega > 10$: $V_0(\Omega) \approx 0.080 \cdot \Omega^{-1.28}$, $V_2(\Omega) \approx 0.187 \cdot \Omega^{-1.43}$. The inset shows $V_{0,2}(\Omega)$ at small values of Ω

The mean value of the parameter R_1, averaged over the uniform distribution of lipid bilayers' directions can be obtained by substituting the angle-dependent coefficients in Equation (19) by their average values corresponding to the random distribution of directions, resulting in the following expression:

$$R_{1\,aver} = \frac{16\,\lambda}{15} \cdot \left[V_0(\Omega) + 4 \cdot V_0(2\Omega) + 3 \cdot V_2(\Omega) + 12 \cdot V_2(2\Omega) \right] \quad (21)$$

Equation (19) can also be used to calculate an average R_1 for a *bundle of parallel axons* (i.e., WM tracks) with the main axis tilted by an angle β with respect to the external magnetic field $\mathbf{B}_0$. In this case, the normal to bilayers within the axon varies remaining perpendicular to the main axonal axis. Assuming a cylindrical axonal shape, by averaging Equation (19) with respect to this variation, we can obtain the following expression for R_1 of a WM track:

$$R_{1,axon} = \frac{\lambda}{2} \cdot \left[\sin^2 \beta \cdot (5 + 3 \; \cos 2\beta) \cdot V_0(\Omega) \right.$$
$$+ \left(16 \; \cos^2 \beta + 6 \cdot \sin^4 \beta\right) \cdot V_0(2\Omega) +$$
$$+ \left(8 - 3 \; \sin^4 \beta\right) \cdot V_2(\Omega)$$
$$\left. + \left(8 + 24 \; \sin^2 \beta + 3 \; \sin^4 \beta\right) \cdot V_2(2\Omega) \right] \quad (22)$$

Equations (19) and (22) reveal an anisotropy of the longitudinal relaxation parameter R_1 in single flat bilayers and in the axonal bundles with respect to their orientation in the magnetic field $\mathbf{B}_0$. To illustrate this anisotropy,

FIGURE 3 The dependence of the ratio $R_1/R_{1\ aver}$ on the angle α between a bilayer and the external field $\mathbf{B}_0$ (left panel) and on the angle β between the axonal bundle axis and $\mathbf{B}_0$ (right panel) for several values of the parameter Ω
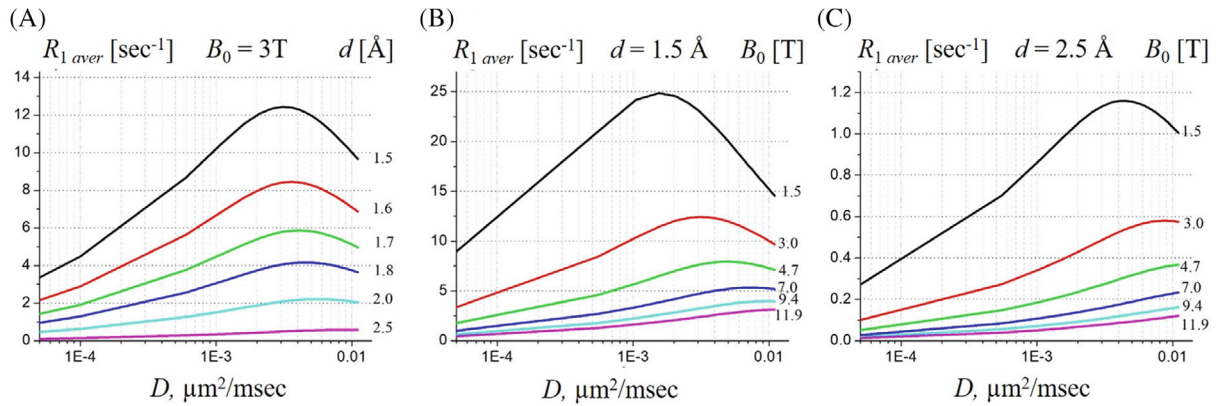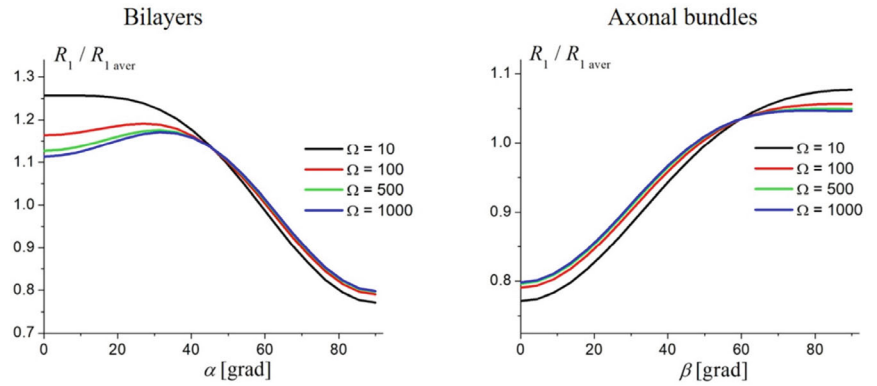

FIGURE 4 The dependence of the mean longitudinal relaxation rate parameter $R_{1,\ aver}$ on the diffusion coefficient D for different values of d (shown by numbers near the lines) at $B_0 = 3$T (A), for different B_0 (shown by numbers near the lines) at $d = 1.5$Å (B), and different B_0 at $d = 2.5$Å (C)

in Figure 3 the ratio $R_1/R_{1\ aver}$ is plotted as a function of bilayer (α) and axonal bundle (β) orientations with respect to the direction of $\mathbf{B}_0$ for several values of Ω. For higher Ω, these dependences become practically independent of Ω. Note also that all the lines corresponding to different values of Ω cross each other at certain angle α or β: $\alpha \approx 45°$ in the case of flat bilayers and $\beta \approx 60°$ in the case of axonal bundles.

The R_1 dependence on the lateral diffusion coefficient D and the distance of the nearest approach d is illustrated in Figure 4 for a range of $D = 0.5 \cdot 10^{-4} - 10^{-2}\ \mu m^2/msec$, and $d = 1.5–2.5$ Å. The surface density was estimated as $n_2 = 1/d^2$. In Figure 4A, the mean relaxation rate parameter $R_{1\ aver}$, Equation (21), is plotted as a function of the diffusion coefficients D for different values of d (shown by numbers near the lines) at $B_0 = 3$T ($\omega_0 = 8 \cdot 10^8\ sec^{-1}$).

Figure 4B and C illustrate the dependence $R_{1\ aver} = R_{1\ aver}(D)$ for different values of the external field B_0 (shown by numbers near the lines) for two values of the parameter d ($d = 1.5$ Å and $d = 2.5$ Å). A non-monotonic dependence of R_1 on the diffusion coefficient D should be noted. It is a result of the trade-off between the decrease of

the coefficient λ and the increase of the functions $V_{0,2}(\Omega)$ with D increasing.

4.2 | Spin–Spin (Transverse) Relaxation of Bound Protons in Lipid Bilayers

In the framework of the classical theory of dipole–dipole relaxation,[33,34] the transverse relaxation parameter R_2 is defined by Equation (8). The spectral densities $J^{(1)}(\omega)$ and $J^{(2)}(2\omega)$ in Equation (8) are the same as analyzed above. However, the integral in Equation (9) for $J^{(0)}(0)$ in the system under consideration diverges due to a slow time decay of the correlation function. To resolve this problem, we should take into account that the Fourier transform in Equation (9) is an approximation (e.g., Ref.[34] Chapter VIII) that is valid only for a sufficiently fast decaying correlation functions. Therefore, the integral for the spectral density $J^{(0)}(0) \equiv J^{(0)}(\omega = 0)$ should be replaced by a time-dependent function $\widetilde{J}^{(0)}(0,\ t)$:

$$J^{(0)}(\omega = 0) \rightarrow \widetilde{J}^{(0)}(0, t) = 2 \cdot \int_0^t d\tau\ G^{(m)}(\tau) \quad (23)$$

Thus, the relaxation parameter R_2 becomes time-dependent,

$$R_2 \rightarrow R_2(t) = \frac{9}{32} \cdot \left(\hbar\gamma^2\right)^2$$
$$\cdot \left\{ \tilde{J}^{(0)}(0, \ t) + 10 \cdot J^{(1)}(\omega) + J^{(2)}(2\omega) \right\}, \quad (24)$$

and the equation for the transverse magnetization $M_\perp(t)$ takes the form:

$$\frac{dM_\perp(t)}{dt} = -R_2(t) \cdot M_\perp(t) \quad (25)$$

Hence, the decay of the transverse magnetization can be described in terms of the relaxation function $\Gamma(t)$,

$$M_\perp(t) = M_\perp(0) \cdot \exp[-\Gamma(t)]$$
$$\Gamma(t) = 2 \cdot \int_0^t d\tau \int_0^\tau d\tau_1 \ G^{(0)}(\tau_1) \quad (26)$$

Substituting the correlation function $G^{(0)}(\tau)$, Equation (14), into Equation (26), the relaxation function $\Gamma(t)$ takes the form:

$$\Gamma(t) = R_2(t, \alpha) \cdot t$$
$$R_2(t, \alpha) = 2\lambda \cdot \left[\left(1 - 3\cos^2\alpha\right)^2 \cdot g_0(\varepsilon) + \frac{9}{2} \cdot \sin^4\alpha \cdot g_2(\varepsilon) \right];$$
$$\varepsilon = t/\tau_d, \quad \tau_d = d^2/2D \quad (27)$$

where we introduced an anisotropic time-dependent relaxation rate function $R_2(t, \alpha) = \Gamma(t, \alpha)/t$, which is a time-dependent analog of a common transverse relaxation rate parameter. The second and third terms in Equation (24) are much smaller than the first term

and, therefore, are omitted in Equation (27). The coefficient λ is given in Equation (20), and the functions $g_{0,2}(\varepsilon)$ are

$$g_{0,2}(\varepsilon) = \int_0^\infty dx \cdot u_{0,2}(x, \ \varepsilon)$$
$$u_{0,2}(x, \ \varepsilon) = x \cdot \left[1 - \frac{1 - \exp\left(-\varepsilon \cdot x^2\right)}{\varepsilon \cdot x^2} \right] \cdot \psi_{0,2}^2(x) \quad (28)$$

The integral in Equation (28) can be calculated only numerically. However, the following analytical representation can be obtained for the experimentally realistic times t corresponding to $\varepsilon \gg 1$:

$$g_0(\varepsilon) = \frac{1}{2} \cdot \ln\varepsilon - \frac{\kappa_0}{2} + 2 \cdot \sqrt{\frac{\pi}{\varepsilon}} + O\left(\frac{\ln\varepsilon}{\varepsilon}\right) \quad (29)$$

$$g_2(\varepsilon) = \frac{1}{9} \cdot \left(\kappa_2 - \frac{\ln\varepsilon}{2\varepsilon}\right) + O\left(\varepsilon^{-1}\right) \quad (30)$$

where the numerical coefficients (rounded to two decimal places) are: $\kappa_0 = 3.20$, $\kappa_2 = 0.75$. The parameter λ, Equation (20), and the functions $g_{0,2}(\varepsilon)$ along with their asymptotic expressions, Equations (29) and (30), are shown in Figure 5.

Since the characteristic diffusion time τ_d is in a nanosecond range, for any realistic time of interest, the ratio $t/\tau_d > 100$. Hence, the function $g_0(\varepsilon)$ can be well approximated by the three first terms in Equation (29) (green line in Figure 5B), and $g_2(\varepsilon)$ can be approximated by its limiting value 0.083. Thus, the relaxation of the transverse magnetization $M_\perp(t)$ is, in general, non-linear-exponential, and in the time interval
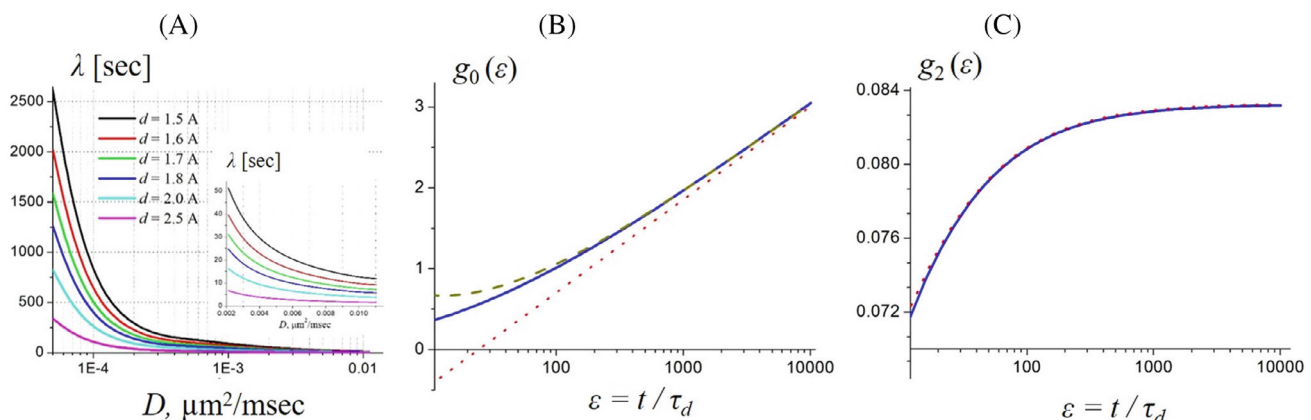

(A)   (B)   (C)

FIGURE 5 A, The dependence of the parameter λ, Equation (20), on the diffusion coefficient D for different inter-proton distances of the closest approach d. B, The function $g_0(\varepsilon)$ (blue line); the red dotted and green dashed lines correspond to the asymptotic expression, Equation (29), with two and three terms included, respectively. C. The functions $g_2(\varepsilon)$ (blue line); the red dotted line corresponds to the asymptotic expression, Equation (30).

$t/\tau_d > 100$ can be described by the following relaxation rate function

$$
R_2(t, \alpha) = \lambda \cdot \left\{ \left(1 - 3\cos^2\alpha\right)^2 \right.
$$
$$
\left. \cdot \left[\ln\left(\frac{t}{\tau_d}\right) - \kappa_0 + 4 \cdot \left(\frac{\pi\,\tau_d}{t}\right)^{1/2} \right] + \kappa_2 \cdot \sin^4\alpha \right\}
$$
(31)

For a special case of the magic angle ($\cos^2\alpha_m = 1/3$), the relaxation rate function becomes time-independent and reduces to $R_2\,(t,\, \alpha = \alpha_m) = 4\kappa_2\lambda/9$. However, for α not too close to α_m, the last term is much smaller than the combination of the first three terms and gives only a small contribution to $R_2(t,\, \alpha)$.

Note that only the last two terms in Equation (8) depend on the magnitude of the external field B_0, while the first one considered here does not. Since these two terms are much smaller than the first one, their contribution to $R_2(t,\, \alpha)$ is very small. Hence, the dependence of R_2 on the external field B_0 is very weak and is not considered herein.

Since the relaxation rate function R_2 depends on time t, the transverse relaxation time T_2 cannot be defined simply as $1/R_2$. Instead, we can introduce T_2 as a time, by which the transverse magnetization has decreased e-fold. This apparent T_2 is a solution of the transcendent equation

$$
R_2\,(T_2, \alpha) \cdot T_2 = 1
$$
(32)

The dependence of the transverse relaxation time T_2 on the diffusion coefficient D at different values of inter-proton distances d is shown in Figure 6 for three orientations of the plane with respect to the external field $\mathbf{B}_0$: $\alpha = 0$, $\alpha = \pi/2$, and for the magic angle $\alpha = \alpha_m$.

4.3 | LDM Absorption Lineshape

In this section, we discuss the absorption lineshape corresponding to the transverse magnetization $M_\perp(t)$ obtained in the previous sections, Equation (26). For a single bilayer forming an angle α with magnetic field $\mathbf{B}_0$ (Figure 1), the frequency dependence of the lineshape $L(\Delta\omega, \alpha)$ is described by a Fourier transform of $M_\perp(t)$ in Equation (26):

$$
L(\Delta\omega,\;\alpha) = \frac{1}{\pi} \cdot \int_0^{+\infty} dt\; \frac{M_\perp(t)}{M_\perp(0)}\;\cos(\Delta\omega \cdot t)
$$
$$
= \frac{1}{\pi} \cdot \int_0^{+\infty} dt\;\exp\left[-t \cdot R_2(t,\alpha)\right] \cdot \cos\Delta\omega \cdot t
$$
(33)

where $R_2(t, \alpha)$ is defined by a general Equation (27) with a long-time asymptotic in Equation (31). For a special case of the magic angle α_m, the relaxation rate function, $R_2\,(t, \alpha = \alpha_m) = 4\kappa_2\lambda/9$, does not depend on time t, and $L\,(\Delta\omega,\, \alpha_m)$ reduces to a standard Lorentzian form:

$$
L\,(\Delta\omega,\, \alpha_m) = \frac{1}{\pi} \cdot \frac{4\kappa_2\lambda/9}{\Delta\omega^2 + (4\kappa_2\lambda/9)^2}
$$
(34)

In the general case $\alpha \neq \alpha_m$, the relaxation rate function $R_2(t,\,\alpha)$ depends on time t in a rather complicated way, and an analytical closed expression for the function $L(\Delta\omega,\,\alpha)$ is unavailable. However, for realistic experimental conditions typical for MT experiments, the frequency offset
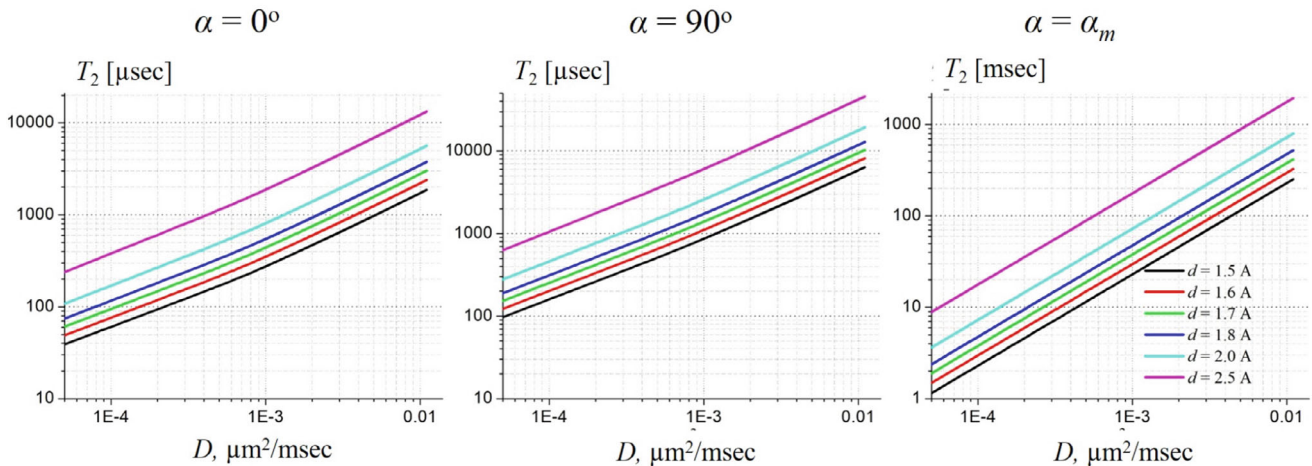

FIGURE 6 The dependence of the transverse relaxation time T_2 on the diffusion coefficient D at different values of inter-proton distances d for $\alpha = 0$, $\alpha = \pi/2$, and for the magic angle $\alpha = \alpha_m(\cos^2\alpha_m = 1/3)$. Note a different T_2 time scale and the units (ms vs. μs) for the magic angle
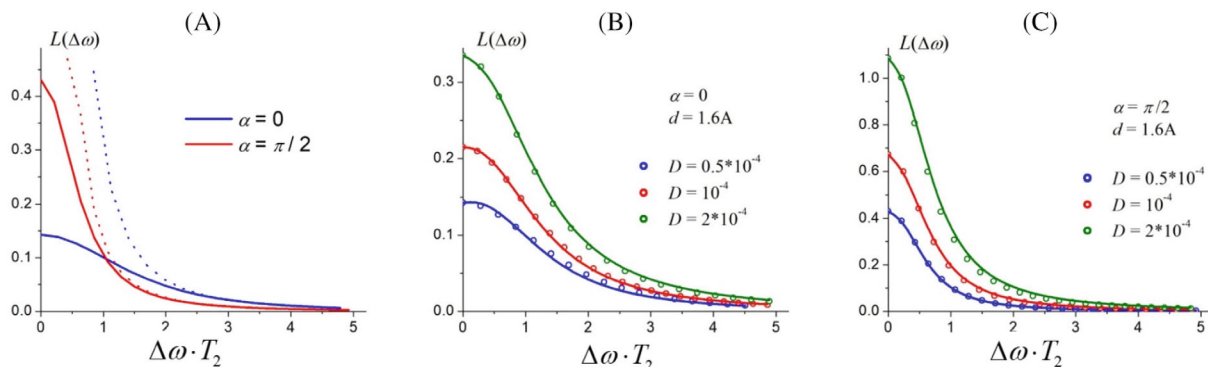
FIGURE 7 Numerically calculated lineshape function $L(\Delta\omega, \alpha)$ (solid lines) and its approximations. A, High-frequency approximation (dashed lines), Equation (35), $d = 1.6$Å, $D = 0.5 \cdot 10^{-4}$ $\mu m^2/$msec. B,C, Interpolation expressions (symbols), Equation (37), $d = 1.6$ Å, $\alpha = 0$ and $\alpha = \pi/2$, and different values of the diffusion coefficient D

$\Delta\omega = 2\pi \cdot \Delta f$ is usually much bigger than the values of the relaxation rate defined as $1/T_2$, and it can be shown that the function $L(\Delta\omega, \alpha)$ tends to the following asymptotic expression:

$$L(\Delta\omega, \alpha) = \frac{\Lambda(\Delta\omega, \alpha)}{\Delta\omega^2}$$

$$\Lambda(\Delta\omega, \alpha) = \frac{\lambda}{2} \cdot \left\{ \left(1 - 3\cos^2 \alpha\right)^2 \cdot \left[\ln\left(\frac{\pi}{4\,\Delta\omega \cdot \tau_d}\right)\right.\right.$$

$$\left.\left. -\kappa_0 + \kappa_1 \cdot (\Delta\omega \cdot \tau_d)^{1/2}\right] + \kappa_2 \cdot \sin^4 \alpha \right\} \quad (35)$$

with the numerical coefficients $\kappa_0 = 3.20$, $\kappa_2 = 0.75$, $\kappa_1 = 12 - 4\sqrt{2}$. The correspondence of the numerically calculated $L(\Delta\omega, \alpha)$ and its high-frequency asymptote, Equation (35), is exemplified in Figure 7A for $\alpha = 0$ and $\alpha = \pi/2$ ($d = 1.6$Å, $D = 0.5 \cdot 10^{-4}$ $\mu m^2/$msec). One can see that for $\alpha = 0$, the asymptotic expression in Equation (35) describes the exact shape of the lineshape function $L(\Delta\omega, \alpha)$ rather well if $\Delta\omega \cdot T_2 > 1$, while the case $\alpha = \pi/2$ requires slightly higher frequencies, $\Delta\omega \cdot T_2 > 2$.

In the opposite case of small $\Delta\omega$, $(T_2 \cdot \Delta\omega) < 1$, Equation (35) is not valid, moreover, in the limit $\Delta\omega \to 0$ it diverges. The two limits of small and large $\Delta\omega$ can be combined together using an interpolation formula:

$$L(\Delta\omega, \alpha) = \frac{\Lambda(\Delta\omega, \alpha)}{\Delta\omega^2 + \Lambda(\Delta\omega, \alpha)/L_0(\alpha)} \quad (36)$$

with $L(\Delta\omega, \alpha)$ defined by Equation (35) and $L_0(\alpha) = L(\Delta\omega = 0, \alpha)$ should be calculated from Equation (33) with $\Delta\omega = 0$ and $R_2(t, \alpha)$ defined by the original Equation (27).

In the case when the angle α is not too close to the magic angle (i.e., the first term in Equation (35) is much bigger than the second one), the function $L_0(\alpha)$ allows the

following expansion:

$$L_0(\alpha) = \frac{1}{\pi\lambda \cdot \left(1 - 3\cos^2 \alpha\right)^2} \cdot$$

$$\left(\frac{1}{\mu} + \frac{\ln\mu - 1 + C}{\mu^2}\right) + O\left(\mu^{-3}\right)$$

$$\mu = \left| \ln\left(\lambda\tau_d \cdot \left(1 - 3\cos^2 \alpha\right)^2\right) \right| \gg 1 \quad (37)$$

while in the case of magic angle, $L_0(\alpha)$ is given by the general formula in Equation (34) (C is the Euler constant).

The lineshape function $L(\Delta\omega, \alpha)$ calculated numerically from Equation (33) and its approximation, Equations (36) and (37), are exemplified in Figure 7B and C for $d = 1.6$ Å, $\alpha = 0$ and $\alpha = \pi/2$, and different values of the diffusion coefficient D.

While the results presented above provide information on protons' spin–spin relaxation in "flat" bilayers (as shown in Figure 1), in biological tissues these bilayers are organized in cellular membranes and myelin sheath.

In the case of *uniformly distributed orientations* of the main axis of the lipid chains with respect to the magnetic field $\mathbf{B}_0$, the absorption lineshape averaged over α can be presented as

$$\bar{L}(\Delta\omega) = \int_0^{\pi/2} \sin\alpha \, d\alpha \, L(\Delta\omega, \alpha)$$

$$= \int_0^{\pi/2} \sin\alpha \, d\alpha \cdot \frac{\Lambda(\Delta\omega, \alpha)}{\Delta\omega^2 + \Lambda(\Delta\omega, \alpha)/L_0(\alpha)} \quad (38)$$

It can be readily verified that the function $\bar{L}(\Delta\omega)$ has a typical sharp maximum at $\Delta\omega \to 0$ characteristic to super-Lorentzian (SL) lineshape function and, therefore, can be referred to as "pseudo"-SL (pSL). Note, however, in contrast to the commonly used SL lineshape based on the Gaussian or Lorentzian distributions (e.g., Refs.[2,5,35–37]),

the function pSL $\overline{L}(\Delta\omega)$ remains finite at $\Delta\omega \to 0$ due to the term proportional to κ_2 in $R_2(t, \alpha)$ and would diverge at $\Delta\omega \to 0$ without it. For large $\Delta\omega$, the lineshape function, Equation (38), can be calculated based on Equation (35), resulting in the following equation:

$$\overline{L}(\Delta\omega) = \frac{2\lambda}{5(\Delta\omega)^2} \cdot \left\{ \ln\left(\frac{\pi}{4\,\Delta\omega \cdot \tau_d}\right) + \kappa_1 \cdot (\Delta\omega \cdot \tau_d)^{1/2} \right.$$
$$\left. -\kappa_0 + \frac{2}{3}\kappa_2 \right\}, \quad \Delta\omega \cdot T_2 > 1 \tag{39}$$

Another important case represents a *bundle of parallel axons* (i.e., WM tracks) with the main axis tilted by an angle β with respect to the external magnetic field $\mathbf{B}_0$. In this case, the normal to bilayers within the axon varies remaining perpendicular to the main axonal axis. Assuming a cylindrical axonal shape, by averaging Equation (33) with respect to this variation, we can obtain a general expression for the axonal bundle lineshape. For large frequency shifts $\Delta\omega \cdot T_2 > 1$ this expression becomes as follows:

$$L_{axon}(\Delta\omega, \beta) = \frac{\lambda}{2(\Delta\omega)^2} \cdot \left\{ \left[\ln\left(\frac{\pi}{4\,\Delta\omega \cdot \tau_d}\right) \right. \right.$$
$$\left. -\kappa_0 + \kappa_1 \cdot (\Delta\omega \cdot \tau_d)^{1/2} \right] \cdot \left(\frac{27}{8}\left(\cos^2\beta - \frac{5}{9} \right)^2 + \frac{1}{3} \right) +$$
$$\left. +\kappa_2 \cdot \left(\cos^2\beta + \frac{3}{8} \cdot \sin^4\beta \right) \right\} \tag{40}$$

5 | DISCUSSION

Deciphering salient features of biological tissue cellular microstructure in healthy organs and the microstructural changes in diseases is an ultimate goal of MRI. While most MRI approaches are based on studying MR properties of "free" water that is abundant in biological tissues, they can only provide indirect information on the tissue cellular structure. Other MRI approaches with off-resonance RF excitation, such as MT[2,5,7,38,39] and inhomogeneous MT (ihMT),[6,40,41] as well as with on-resonance RF excitation that are based on gradient echo sequences,[9–11] chemical exchange,[12] inversion recovery,[13] SMART,[14] and UTE MRI,[2,15–17] – provide more direct access to cellular microstructure because they target MRI signals originated directly from protons bound to biological-tissue-forming macromolecules. However, despite of three decades of successful applications, interpretation of these experiments is still based on assumed phenomenological parameters (including bound protons T_1 and T_2 relaxation properties), whereas the relationship between these parameters and cellular structure is still not known. This hampers not only

interpretation of experimental results but also designing new experiments targeting macromolecular signals.

In the present study, we provide a theoretical analysis of the spin–spin and spin–lattice relaxation properties of the protons bound to the lipid chains within cellular membranes and the myelin sheath. Up to our best knowledge, this is the first analytical theory establishing a dependence of the transverse (spin–spin) and longitudinal (spin–lattice) relaxation times of lipid-chain-bound protons and cellular membranes on the myelin sheath molecular structure and dynamic properties. We have established a contribution to the bound protons relaxation properties of the dipole–dipole interaction between proton spins modulated by the lateral diffusion of the macromolecules "dragging along" protons of the alkyl chains in methylene groups. We derived quantitative analytical equations showing how the bound protons T_1 and T_2 relaxation mechanisms depend on the lateral diffusion coefficient D and the distance of the proton-proton nearest approach d. Our results are in a qualitative agreement with direct analysis of myelin proton spectrum (e.g.,[1,2]) that revealed a presence of bound pool protons with T_2 ranging between 10 and 100 μs.

While direct measurements of T_2 in lipid and myelin membranes are limited,[1,2] a number of indirect estimates were presented in the literature (see for example, Refs.[2,5–7,14,19,38–41]) following pioneering work of Morrison and Henkelman[5] who proposed a basic exchange model describing MT experiments. However, due to the complexity of biological system, even this basic model inevitably relied on quite a few phenomenological parameters that were not available from experimental data and had to be assumed for estimating T_2 of bound protons. For example, T_1 of bound protons was assumed to be equal to 1 s and independent of their location in the cellular structure. Under this assumption, the T_2 of bound protons was estimated as 10.4 μs supposing SL lineshape, 18 μs supposing Gaussian lineshape and 230 μs supposing Lorentzian lineshape. The assumption of a 1 s T_1 and a SL lineshape became since then a broadly accepted paradigm for interpretation of MT experiments. However, it worth noting that several SL compartments were required to explain direct T_2 measurements by Wilhelm et al.[2] It also worth noting that the assumption of the same T_1 but distribution of T_2s described by the SL model is, to some extent, contradictory. Indeed, the nature of SL distribution is rooted in the Wennerstrom theory[35,36] that explains distribution of bound protons T_2s by the distribution of the orientations of lipid membranes. Our theory shows that such a distribution of lipid membranes orientations also leads to a distribution of bound protons T_1s that can potentially be incorporated in the analysis of MT data.

Our approach is based on the classical theory of dipole–dipole relaxation,[33,34] where the relaxation parameters $R_{1,2}$ are determined by the spectral densities $J^{(m)}(\omega)$, which are the Fourier transforms of the correlation functions $G^{(m)}(\tau)$, Equations (7) and (8). In the case of 3D diffusion, the latter decrease with τ as $G^{(m)}(\tau) \sim \tau^{-3/2}$ at $\tau \gg \tau_d$ (τ_d is the characteristic diffusion time),[33,34] and the integrals defining the Fourier transforms converge at any ω. This behavior is different in our case of the 2D diffusion, where $G^{(m)}(\tau) \sim \tau^{-1}$. As discussed above, in this case one of the spectral densities, $J^{(0)}(0)$, entering Equation (8) for the transverse relaxation, does not exist and was replaced in our approach by a time-dependent quantity $\widetilde{J}^{(0)}(0, \ t)$, Equation (23).

The spin–lattice (longitudinal) relaxation is defined by the spectral densities $J^{(1,2)}(\omega)$ at non-zero frequencies, for which the Fourier transforms of $G^{(1,2)}(\tau)$ are well defined. Hence, they were calculated in a regular way without involving a time-dependent spectral densities. Our results presented in Figure 4 demonstrate how the R_1 relaxation of bound protons depends on the model parameters – the lateral diffusion coefficient D, the parameter d defining the distance of the closest approach between diffusing protons. The results also show the R_1 dependence on the strength of the external field B_0. In particular, it is shown that R_1 decreases with B_0 increases, qualitatively similar to that predicted and analyzed by Schyboll et al[20] but with a sharper decrease with B_0 increase ($R_1 \sim B_0^{-1.3}$ in our LDM theory, versus, $R_1 \sim B_0^{-0.45}$ found in[20]). The LDM predicts that depending on the values of parameters D, d, and B_0, the T_1 relaxation time ($T_1 = 1/R_1$) can vary in the range of 100 μs to a few seconds, that is in the range of values found in phospholipids membranes.[42–45] The dependence of R_1 on the diffusion coefficient D is not monotonic and has a maximum at $D \approx 3 \cdot 10^{-3} \ \mu m^2/msec$.

It is important to note that the LDM predicts an anisotropic behavior of R_1 in bilayers and axonal bundles, that is, the R_1 dependence on the bilayers' and bundles' orientation with respect to the external magnetic field $\mathbf{B}_0$. The results show that the mean R_1 relaxation of axonal bundles with the main axis parallel to the magnetic field $\mathbf{B}_0$ is about 30% smaller than the R_1 of axonal bundles perpendicular to $\mathbf{B}_0$. For bilayers, the perpendicular orientation of their normal to $\mathbf{B}_0$ results in the smallest R_1, besides, the R_1 angular dependence is not monotonic, reaching a maximum around 30–40^0 from $\mathbf{B}_0$, followed by a shallow minimum for the parallel orientation. While there are no known to us direct measurements of R_1 anisotropy of lipid-bound protons, the report on free water measurement in WM showed increased R_1 relaxation rate for nerve bundles oriented perpendicular to $\mathbf{B}_0$ as compared with bundles oriented parallel to $\mathbf{B}_0$, as observed in healthy subjects investigated at 3 T.[46]

The properties of the spin–spin relaxation are substantially different - the relaxation function $\Gamma(t) = -\ln\left[M_\perp(t)/M_\perp(0)\right]$, describing the transverse relaxation of lipid-bound protons in bilayers is not linear in time t: $\Gamma(t) = R_2(t) \cdot t$. As the quantity $R_2(t)$ depends on time t, it cannot be referred to as a "relaxation rate constant", instead we call it a relaxation rate function. Importantly, the main contribution to the transverse relaxation rate function $R_2(t) \sim \ln t$, Equation (31), with the proportionality coefficient strongly orientation dependent, nulling at the magic angle orientation. This logarithmic $R_2(t)$ behavior is intermediate between the case of unrestricted diffusion,[33,34] where R_2 is a constant (does not depend on time), and the case of fully restricted diffusion proposed by Furman et al,[47] where the relaxation was described by a Gaussian-type function, that is, $\Gamma(t) \sim t^2$. It can be readily verified that in another "intermediate" case–1D diffusion–the relaxation function $\Gamma(t) \sim t^{3/2}$ and, correspondingly, $R_2(t) \sim t^{1/2}$.

It is important to note that the values of the transverse relaxation function $R_2(t)$ of the lipid-bound protons in bilayers are several orders of magnitude bigger than those of R_1. Also, in contrast to R_1, the relaxation function $R_2(t)$ has a very weak dependence on the external field B_0. Similar to R_1, the relaxation function $R_2(t)$ also vary significantly as a function of the lateral diffusion coefficient D and the parameter d defining the distance of closest approach between diffusing protons. Since the transverse relaxation function $R_2(t)$ depends on time, the transverse signal decay cannot be characterized by a single time-independent parameter similar to $T_1 = 1/R_1$. Instead, to characterize transverse relaxation, we have introduced an *apparent transverse relaxation time parameter* T_2 defined as a time, by which the transverse magnetization has reduced e times, Equation (32). The results presented in Figure 6 show that this apparent T_2 relaxation time parameter also varies significantly as a function of the lateral diffusion coefficient D, the parameter d, and the membranes' orientation with respect to the external magnetic field (*anisotropic effect*). The T_2 can vary between 10 μs to a few seconds, being especially long for the case of the magic angle orientation. The shortest T_2 is achieved for slow lateral diffusion ($D \sim 0.5 \cdot 10^{-4} \mu m^2/ms$) and smaller parameter d ($d \sim 1.5$A).

In addition to the time dependence of the transverse relaxation function $R_2(t)$ of the lipid-bound protons in bilayers, the LDM also predicts the $R_2(t)$ orientation dependence that is in agreement with experimental data. Indeed, the LDM-predicted angular dependence of the relaxation function $R_2(t)$ in flat bilayers ($(1 - 3\cos^2\alpha)^2$ per Equation (31)) is similar to that found experimentally by Morris et al.[48] Indeed, Morris et al measured the orientation dependence of the second moment (M_2)

of the lineshape in an oriented phospholipid bilayer at 9.4T. They found a strong orientation dependence that was maximized when the bilayers were aligned perpendicular to $\mathbf{B}_0$ and minimized near the magic angle ($\sim$54.7°) and followed an orientation dependence given by the second Legendre polynomial squared. Also, the LDM predicted strong anisotropy of T_2 relaxation in WM is in agreement with the previous MT-based discovery of Pampel et al.[39] The authors[39] found a distinct correlation between the diffusion-tensor orientation with respect to the $\mathbf{B}_0$-magnetic field and the apparent transverse relaxation time, T_2, of the semisolid pool (i.e., the width of its absorption line). This orientation dependence was quantitatively explained by a refined dipolar lineshape that explicitly considered the specific geometrical arrangement of lipid bilayers wrapped around a cylindrical axon, which is similar to our axonal model in Equation (40).

The important features of $R_2(t)$ behavior outlined above, might have important implications for interpretation of MT experiments. Traditionally, MT results are analyzed based on the so-called SL absorption lineshape, proposed by Wennerstrom[35,36] for randomly distributed membranes directions and the analysis of the secular part of the dipole–dipole Hamiltonian that has a $\left(1 - 3\cos^2\alpha\right)$ membranes orientation dependence. The Wennerstrom's approach leads to a SL lineshape $L_{SL}(\Delta\omega)$:

$$L_{SL}(\Delta\omega) = \int_0^1 \frac{dx}{|3x^2 - 1|} \cdot f\left(\frac{\Delta\omega}{R_2 \cdot |3x^2 - 1|}\right), \quad x = \cos\alpha$$
(41)

where $f(.)$ is a normalized function, usually assumed Gaussian or Lorentzian, and R_2 is a phenomenological relaxation rate parameter. It is interesting to note that the assumption that the projections of all proton-proton vectors in the dipole–dipole Hamiltonian on the membrane's plane (in our case, xy-plane) average to zero, made in,[35,36] is "opposite" to our approach that considers interactions between protons located in the neighboring lipid macromolecules. The time-dependence of the relaxation function $R_2(t, \alpha)$ lead to more complicated LDM-defined absorption lineshapes, Equations (35)–(40), than in Equation (41). Consequently, for uniformly distributed orientations of bilayers, the global absorption lineshape is referred to here as a "pseudo-Super-Lorentzian", or pSL. Though both SL and pSL have the same hallmark–a very sharp maximum at $\Delta\omega \to 0$, – there are several differences between them. First, the integrand in Equation (38) (the LDM analog of Equation 41) is the well-defined angle-dependent pseudo-Lorentzian function $L(\Delta\omega, \alpha)$ from Equation (37). In addition, in contrast to the SL lineshape $L_{SL}(\Delta\omega)$, the pSL lineshape remains finite at $\Delta\omega \to 0$ due to the term proportional to the coefficient κ_2, which plays an important role in the vicinity of the magic angle.

The LDM-defined lineshape function for axonal bundles, Equation (40), predicts anisotropic behavior with respect to the axonal orientation with $\mathbf{B}_0$.

6 | CONCLUSIONS

In the present study, we have introduced the LDM that microscopically relates longitudinal and transverse relaxation properties of protons bound to the lipid chains forming cellular and myelin membranes to the lipid chains' structure and diffusional dynamic. Our results predict that:

a. The transverse relaxation of bound protons cannot be described in terms of a commonly used R_2 relaxation rate parameter. Instead, LDM approach describes transverse relaxation in terms of a transverse relaxation rate function $R_2(t, \alpha)$ that in the main approximation has a logarithmic behavior with respect to the time t after the RF excitation pulse: $R_2(t, \alpha) \sim \ln t$.

b. T_1 (spin–lattice) and T_2 (spin–spin) relaxation properties of bound protons in cellular and myelin membranes are highly anisotropic, that is, they depend on the orientations of the membranes with respect to the external magnetic field $\mathbf{B}_0$.

c. The anisotropic non-linear transverse relaxation of bound protons leads to a pSL global lineshape that is different from an SL lineshape commonly used in interpreting MT and ihMT experiments. For bundles of parallel axons (WM tracks), the pSL lineshape is anisotropic, that is, depends on the axonal direction with respect to the external magnetic field $\mathbf{B}_0$.

ORCID
Dmitriy A. Yablonskiy https://orcid.org/0000-0003-2898-8797

REFERENCES

1. Horch RA, Gore JC, Does MD. Origins of the ultrashort-T2 1H NMR signals in myelinated nerve: a direct measure of myelin content? *Magn Reson Med*. 2011;66:24-31.
2. Wilhelm MJ, Ong HH, Wehrli SL, Li C, Tsai PH, Hackney DB, Wehrli FW. Direct magnetic resonance detection of myelin and prospects for quantitative imaging of myelin density. *Proc Natl Acad Sci U S A*. 2012;109:9605-9610.
3. Wolff SD, Balaban RS. Magnetization transfer contrast (MTC) and tissue water proton relaxation in vivo. *Magn Reson Med*. 1989;10:135-144.
4. Henkelman RM, Huang X, Xiang QS, Stanisz GJ, Swanson SD, Bronskill MJ. Quantitative interpretation of magnetization transfer. *Magn Reson Med*. 1993;29:759-766.

5. Morrison C, Henkelman RM. A model for magnetization transfer in tissues. *Magn Reson Med*. 1995;33:475-482.

6. Varma G, Girard OM, Prevost VH, Grant AK, Duhamel G, Alsop DC. Interpretation of magnetization transfer from inhomogeneously broadened lines (ihMT) in tissues as a dipolar order effect within motion restricted molecules. *J Magn Reson*. 2015;260:67-76.

7. Sled JG. Modelling and interpretation of magnetization transfer imaging in the brain. *Neuroimage*. 2018;182:128-135.

8. Kisel AA, Naumova AV, Yarnykh VL. Macromolecular Proton Fraction as a Myelin Biomarker: Principles, Validation, and Applications. *Front Neurosci*. 2022;16:819912.

9. Pike GB. Pulsed magnetization transfer contrast in gradient echo imaging: a two-pool analytic description of signal response. *Magn Reson Med*. 1996;36:95-103.

10. Ou X, Gochberg DF. MT effects and T_1 quantification in single-slice spoiled gradient echo imaging. *Magn Reson Med*. 2008;59:835-845.

11. Gloor M, Scheffler K, Bieri O. Quantitative magnetization transfer imaging using balanced SSFP. *Magn Reson Med*. 2008;60:691-700.

12. Zaiss M, Zu Z, Xu J, et al. A combined analytical solution for chemical exchange saturation transfer and semi-solid magnetization transfer. *NMR Biomed*. 2015;28:217-230.

13. Prantner AM, Bretthorst GL, Neil JJ, Garbow JR, Ackerman JJ. Magnetization transfer induced biexponential longitudinal relaxation. *Magn Reson Med*. 2008;60:555-563.

14. Sukstanskii AL, Wen J, Cross AH, Yablonskiy DA. Simultaneous multi-angular relaxometry of tissue with MRI (SMART MRI): Theoretical background and proof of concept. *Magn Reson Med*. 2017;77:1296-1306.

15. Du J, Ma G, Li S, et al. Ultrashort echo time (UTE) magnetic resonance imaging of the short T2 components in white matter of the brain using a clinical 3T scanner. *Neuroimage*. 2014; 87:32-41.

16. Du J, Sheth V, He Q, et al. Measurement of T_1 of the ultrashort T_2^* components in white matter of the brain at 3T. *PLoS One*. 2014;9:e103296.

17. Boucneau T, Cao P, Tang S, et al. In vivo characterization of brain ultrashort-T2 components. *Magn Reson Med*. 2018;80:726-735.

18. Does MD. Inferring brain tissue composition and microstructure via MR relaxometry. *Neuroimage*. 2018;182:136-148.

19. Brown MF. Theory of spin-lattice relaxation in lipid bilayers and biological membranes. *Dipolar relaxation J Chem Phys*. 1984;80:2808-2831.

20. Schyboll F, Jaekel U, Petruccione F, Neeb H. Dipolar induced spin-lattice relaxation in the myelin sheath: A molecular dynamics study. *Sci Rep*. 2019;9:14813.

21. Norton WT, Autilio LA. The lipid composition of purified bovine brain myelin. *J Neurochem*. 1966;13:213-222.

22. Koenig SH. Cholesterol of myelin is the determinant of gray-white contrast in MRI of brain. *Magn Reson Med*. 1991;20:285-291.

23. DeVries GH, Zetusky WJ, Zmachinski C, Calabrese V. Lipid composition of axolemma-enriched fractions from human brains. *J Lipid Res*. 1981;22:208-216.

24. Schoch RL, Brown FLH, Haran G. Correlated diffusion in lipid bilayers. *Proc Natl Acad Sci USA*. 2021;118. doi:10.1073/pnas.213202118

25. Knowles PF, Marsh D. Magnetic resonance of membranes. *Biochem J*. 1991;274:625-641.

26. Kahya N, Schwille P. How phospholipid-cholesterol interactions modulate lipid lateral diffusion, as revealed by fluorescence correlation spectroscopy. *J Fluoresc*. 2006;16:671-678.

27. Machan R, Hof M. Lipid diffusion in planar membranes investigated by fluorescence correlation spectroscopy. *Biochim Biophys Acta*. 2010;1798:1377-1391.

28. Lipid LG, Diffusion L. *In: Roberts GCK, editor*. Encyclopedia of BioPhysics; 2013.

29. Gaede HC, Gawrisch K. Lateral diffusion rates of lipid, water, and a hydrophobic drug in a multilamellar liposome. *Biophys J*. 2003;85:1734-1740.

30. Oshima A, Nakashima H, Sumitomo K. Evaluation of Lateral Diffusion of Lipids in Continuous Membranes between Free-standing and Supported Areas by Fluorescence Recovery after Photobleaching. *Langmuir*. 2019;35:11725-11734.

31. Okamura E. Solution NMR to Quantify Mobility in Membranes: Diffusion, Protrusion, and Drug Transport Processes. *Chem Pharm Bull (Tokyo)*. 2019;67:308-315.

32. Gáspári Z, A. P. Chapter 2 - Protein Dynamics as Reported by NMR2010. 35–75 p.

33. Bloembergen N, Purcell EM, Pound RV. Relaxation Effects in Nuclear Magneic Resonance Absorption. *Phys Rev*. 1948;73:679-712.

34. Abragam A. *Principles of Nuclear Magnetism*. Oxford University Press; 1989.

35. Wennerstrom H. Proton Nuclear Magnetic Resonance Lineshapes in Lammelar liquid Crystals. *Chem Phys Lett*. 1973;18:41-44.

36. Wennerstrom H, Lindblom G. Biological and model membranes studied by nuclear magnetic resonance of spin one half nuclei. *Q Rev Biophys*. 1977;10:67-96.

37. Bloom M, Holmes KT, Mountford CE, Williams PG. Complete Proton Magnetic Resonance in Whole Cells. *J Magn Reson*. 1986;69:73-91.

38. Yarnykh VL. Fast macromolecular proton fraction mapping from a single off-resonance magnetization transfer measurement. *Magn Reson Med*. 2012;68:166-178.

39. Pampel A, Muller DK, Anwander A, Marschner H, Moller HE. Orientation dependence of magnetization transfer parameters in human white matter. *Neuroimage*. 2015;114:136-146.

40. Varma G, Duhamel G, de Bazelaire C, Alsop DC. Magnetization transfer from inhomogeneously broadened lines: A potential marker for myelin. *Magn Reson Med*. 2015;73:614-622.

41. Manning AP, Chang KL, MacKay AL, Michal CA. The physical mechanism of "inhomogeneous" magnetization transfer MRI. *J Magn Reson*. 2017;274:125-136.

42. Daycock J, Darke A, Chapman D. Nuclear relaxation (T1) measurements of lecitin-water systems. *Chem & Phys of Lipids*. 1971;6:205-214.

43. Feigenson GW, Chan SI. Nuclear magnetic relaxation behavior of lecithin multilayers. *J Am Chem Soc*. 1974;96:1312-1319.

44. Cornell BA, Pope JM, Troup GJ. A pulsed N.M.R study of D2O bound to 1,2 dipalmitoyl phosphatidylcholine. *Chem Phys Lipids*. 1974;13:183-201.

45. Deese AJ, Dratz EA, Hymel L, Fleischer S. Proton NMR T_1, T_2, and T_1 rho relaxation studies of native and reconstituted sarcoplasmic reticulum and phospholipid vesicles. *Biophys J*. 1982;37:207-216.

46. Schyboll F, Jaekel U, Weber B, Neeb H. The impact of fibre orientation on T1-relaxation and apparent tissue water content in white matter. *Magnetic Resonance Materials in Physics, Biology and Medicine*. 2018;31:501-510.

47. Furman GB, Meerovich VM, Sokolovsky VL. Correlation of transverse relaxation time with structure of biological tissue. *J Magn Reson*. 2016;270:7-11.

48. Morris SR, Frederick R, MacKay AL, Laule C, Michal CA. Orientation dependence of inhomogeneous magnetization transfer and dipolar order relaxation rate in phospholipid bilayers. *J Magn Reson*. 2022;338:107205.

APPENDIX A

A.1 Table of parameters

B_0–external magnetic field.

α–angle between a normal to bilayer and B_0.

β–angle between an axonal main axis and B_0.

$\hbar$–Planck constant.

γ–gyromagnetic ratio.

I–nuclear spin ($= 1/2$ in our case).

$J^{(m)}(\omega)$ ($m = 0, 1, 2$) – spectral densities.

$\widetilde{J}^{(0)}(0, \ t)$–time-dependent spectral density.

$G^{(m)}(\tau)$ ($m = 0, 1, 2$) - correlation functions.

D–lateral diffusion coefficient.

d–minimal "approachable" distance between dipoles.

$\tau_d = d^2/2D$–characteristic diffusion time.

n_2–surface spin density.

R_1–longitudinal (spin–lattice) relaxation parameter.

$R_{1, aver}$–R_1 averaged over uniform orientation distribution of bilayers.

$R_{1, axon}$–R_1 averaged over orientation distribution of bilayers in an axonal bundle.

$R_2(t)$–time-dependent transverse (spin–spin) relaxation parameter.

$\Gamma(t)$–relaxation function.

T_2–effective transverse relaxation time.

$\Delta\omega$–frequency offset of RF field.

$L(\Delta\omega, \ \alpha)$–absorption lineshape for a single bilayer forming an angle α with B_0

$$L_0(\alpha) = L(\Delta\omega = 0, \ \alpha)$$

$\overline{L}(\Delta\omega)$–lineshape averaged over uniform orientation distribution of bilayers.

$L_{axon}(\Delta\omega, \ \beta)$–lineshape averaged over orientation distribution of bilayers in an axonal bundle.